Quest Journals
Journal of Research in Mechanical Engineering
Volume 12 ~ Issue 2 (Mar. – Apr. 2026) pp: 44-64
ISSN(Online):2321-8185
www.questjournals.org

Research Paper

Cam Follower Dynamic Behaviour Modelling Subjected to Impact and Fatigue Loads

[1] I. O .Nyah *[2] W. A. Akpan [3] C. M. Orazulume [4] E.J. Awaka-Ama [5] V. A. Amba

[1] *Department of Mechanical Engineering, Faculty of Engineering University of Uyo, Akwa Ibom State, Nigeria.*

[2] *Department of Mechanical Engineering, School of Engineering and Engineering Technology, Federal University of Technology, Ikot Abasi, Akwa Ibom State, Nigeria.*

[3] *Department of Electrical and Electronics Engineering, Faculty of Engineering, TopFaith University Mkpatak, Akwa Ibom State, Nigeria.*

[4] *Department of Mechanical Engineering of Mechanical Engineering, Faculty of Engineering University of Uyo, Akwa Ibom State, Nigeria.*

[5] *Department of Mechanical Engineering of Mechanical Engineering, Faculty of Engineering University of Uyo, Akwa Ibom State, Nigeria.*

Abstract
Cam follower systems are usually subjected to impact and fatigue loads during dynamic operation. This necessitated the research which modeled and studied the behavior of this system by adequate analysis to identify the important parameters that affect the cam follower system. To achieve this, the simulation of the cam-follower behavior was conducted using MATLAB Simulink. MATLAB Simulink was chosen due to its robust environment for modeling dynamic systems, its built-in solvers for differential equations, and its capability to visualize the results. Besides, dynamic modeling is essential for understanding the response of the system under different operational conditions, ensuring performance optimization and failure prevention. In this study, three critical dynamic phenomena—no contact, impact, and over-travel—were considered, each representing a unique challenge in cam dynamics. Besides, two data points were marked and labeled with the maximum amplitude of vibration, the point of ten percentage of the maximum after the second impact, and the time at which these events occurred. These data points were used to determine a measure of the impact period for M2 and M3. From results, M2 took 0.02136s (0.20330s – 0.18194s) for the magnitude of vibration to reduce to 10% of the maximum and M3 took 0.007639s (0.18646s – 0.17882s) for the same reduction to occur. The absolute maximum simulated acceleration of M2 and M3 were 167 m/s^2 and 841 m/s^2, or 13 and 67 times greater than the theoretical acceleration at the same location. The upward shifted in magnitude of vibration is a result of the collision of M2 andM3. The periodic nature of the cam-follower system is preserved, but impact forces introduce transient fluctuations, primarily affecting velocity. However, and to enhance the performance of real-time cam-follower applications, selection of an optimal mass can help balance stability and responsiveness, minimizing unwanted oscillations and ensuring precise timing.

Keywords: Behaviour , cam follower, dynamic, fatigue, impact, load, modelling,

*Received 09 Apr., 2026; **R**evised 26 Apr., 2026; **A**ccepted 25 Apr., 2026 © The author(s) 2026.*
P**ublished with open access at **www.questjournas.org

I. Introduction

A cam is a rotating or translating part of the cam follower mechanism that can transmit from one type of motion to another. Cam follower mechanism can be used to transmit regular to irregular motion at a very low cost that is very difficult even at higher costs by using other available sophisticated means.

A cam mechanism usually consists of two moving components, the cam and the follower, which are mounted on a fixed frame. The possible applications of cam mechanisms are almost unlimited, and their shapes have great variety. The shape of a cam depends on the transfer function of the follower.

In general, the classification of cam-follower systems is based on shapes of cams and followers. The basic shapes of a cam are plate cam or a disk cam, wedge cam, cylindrical cam or barrel c and a face cam. In these types of cams, plate cams are commonly used in machines. For this cam, with a given continuous input motion of the cam element, the follower moves forward and backward in a straight line. The basic shapes of the follower comprise four different types, such as a knife-edge follower, flat-face follower, roller follower and a spherical face [1].

For the other way of classification based on the motion of the follower, they are reciprocating (translating) followers and oscillating (rotating) followers, [1]. On the other hand, reciprocating followers are cataloged by the centerline of the follower as the offset cam and the radial cam.

Many other researchers have studied the dynamics of the cam and follower mechanism. [2] offered a dynamic model that takes the spring nonlinearity into account. They also considered the side leakage by solving the governing equations in two dimensions. This led to more computational efforts, but they showed that neglecting the edge effects results in an overestimation of the film thickness. Their findings showed that the high pressure -which is induced at the vicinity of the edge of the cam—inhibits the flow of the lubricant. [3] and [4] investigated thermal effects on the cam-and- follower lubrication by solving the thermo-elasto-hydrodynamics (TEHL) governing equations. They found that the trend of parameters during the cam rotation is like the isothermal condition, but quantitatively the results are significantly different. For example, the film thickness in TEHL is thinner than EHL simulation.

[5] designed an experimental apparatus to investigate the cam and follower lubrication. Using that apparatus, they were able to measure the force and the film thickness, but the mechanism itself was different from the actual cam follower mechanism. In their test rig, a high-speed camera was assembled under a fixed glass disc follower while cam was the rotating element.

Another consideration which has recently attracted the attention of many researchers is the running-in phenomenon. In the running-in period, the asperities are gradually flattened, and friction coefficient is progressively reduced until reaching the steady state. A detailed modeling of running-in phenomenon is derived by [6]**.** This model can estimate the wear volume in rolling/sliding contacts subjected to mixed lubrication, and its findings have been verified experimentally using a disk-on-disk rolling- sliding test rig.[7] numerically and experimentally studied the running-in behaviour in journal bearings. They considered the effect of surface roughness and the interaction of running-in and roughness reduction of asperities.

[8] suggested a lot of variety of cam and follower linkages that a designer or researcher can select based on one's requirements. Cam and follower mechanisms are also used to increase the internal combustion (I.C) engine efficiency by various optimization techniques.

The stress-life method has its advantages of requiring the minimum amount of material properties on fatigue, that is Strength-Number of cycles (S-N) curves of materials. It is mostly used to predict the fatigue life of a part at a low- level stress in comparison to its yield strength.[9] stated that for an application with higher elastic strains, the stress life method was equivalent to a strain life method. One essential piece of the information is to determine the endurance limit of the material. An endurance limit refers to the critical stress value for an infinite fatigue life. In practice, an infinite fatigue life corresponds to an acceptable large number of cycles, more especially greater than 106 cycles. To simplify a fatigue analysis, a dynamic load is usually simplified as a periodical sinusoid to represent the dynamic characteristics of loads. However, for most components involved in machines, external loads are very complicated. Simplified periodical sinusoids have their limitations in characterizing dynamic properties appropriately since frequencies and amplitudes change continuously with respect to time.

In describing a dynamic load for a fatigue analysis, the waveform or shape is not so critical; however, peak values and frequencies of loads are critical. To this end, the maximized stress $\sigma_{max}$and the minimized stress σ_{min}in each loading cycle should be determined to characterize the dynamic change of stress in the cycle. Regarding the impact of static stress level on the fatigue life, a mean stress in a cycle should also be determined. Ranging above and below the mean stress can be modeled to characterize the changing pattern of stress.

A mean stress and alternating stress correlate to the maximized and minimized stresses. Assume that the maximized and minimized stresses are denoted as σ_{max} and σ_{min}, respectively, the mean stress $\sigma_m$and alternating stress $\sigma_a$can be determined as:

$$\delta_{max} = \frac{\delta_{max} + \partial_{min}}{2} \qquad \text{Equation 1}$$

$$\delta_{max} = \frac{\delta_{max} - \partial_{min}}{2} \qquad \text{Equation 2}$$

where σ_m is the mean component of stress and σ_a is the alternating component of stress. As a further note, the mean and alternating stresses will be used to analyze the fatigue cycle of objects in the specified failure criterion. Figure 1 shows some commonly used failure criteria [10].

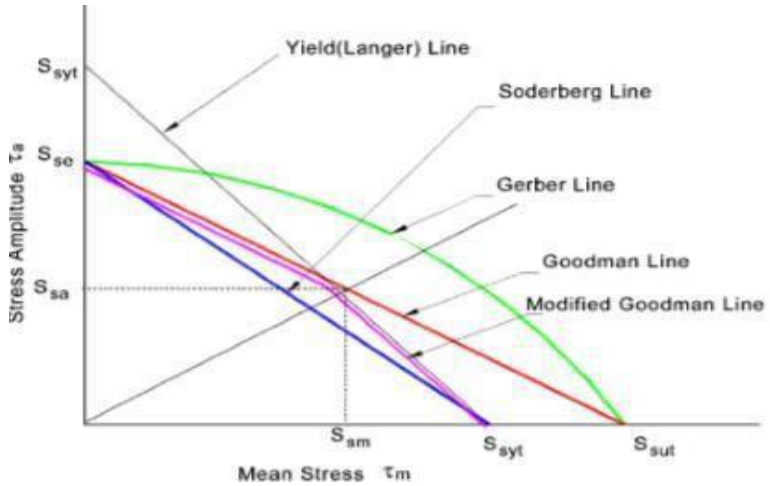

Figure 1: Fatigue Failure Criteria [10]

If there are k levels of stress Si over the give number of cycles, each stress level has a repetitive cycle of ni, and the number of cycles at each stress level is given as Ni, then, the accumulated damage can be determined as in Equation 3 [11].

$$\sum_{N_i}^{n_i} = D \qquad \text{Equation 3}$$

A dynamic load refers to a load that is subjected to change over the time. When objects are in motion there is a dynamic load counts for all types of forces. These include external, inertial, friction and damping forces. In contrast, a static load refers to a load on a structure whose amplitude and direction remain constant over the time. An external load with slow change can be simplified as a static load The dynamic load must be determined to evaluate the variables for fatigue analysis. These variables include mean and alternating stresses, as well as their dependences on time factors. In characterization of a dynamic load, the time is viewed as a reference variable, and the damage growth depends on both of time factor and stress level [12]. Many researchers used the experiments to identify dynamic loads of structures or products. For examples, [13] established a procedure to evaluate dynamic loads and they developed a dynamic model for the testing of wheel drums. [14] evaluated the dynamic loads and performed the fatigue failure on a railway bridge; they used the seismographs that were fixed with tri-axle accelerometers for measurements. An FEA model with 3D beam elements was built to analyze the dynamic behaviors of bridge. In addition, the mean stress effect caused by the weight was considered, and equivalent alternating stress was determined using the Goodman criterion. To characterize a dynamic load, [15] proposed to use a vertically mounted accelerometer to track the engaged force when the vehicle passed over the bumps. The accelerometer was placed at the center of gravity approximately. Quantifying the effect of a dynamic load on a component is not a trivial task. Note that understanding a dynamic load with continuous impact forces is essential to analyze fatigue life of a part.[16] considered the wheel with the real time dynamics of high-speed motion. The wheel rail was involved in the dynamic interaction, and this depended on many factors such as design parameters of wheel and rail, material properties, and contact nonlinearities. of wheel.

Dynamic modeling is a mathematical tool that is used to describe the behaviour of physical systems. These systems may be represented by single or multiple differential equations and may be a mechanical, electrical, thermal, or any other time-varying system. In this case, only dynamic models for mechanical systems are considered. Every real mechanical system has infinite degrees of freedom. The higher the degree of freedom in the model, the more accurate the simulation will be, at the price of model complexity and computation time. To have a reasonable computation time and acceptable results, the model needs to be simplified. This simplification may be done by reducing the degrees of freedom by combining masses, stiffness constants, and damping coefficients. The simplest dynamic model is a single degree of freedom model with one mass, one spring, and one damper. More complex models have multiple degrees of freedom with multiple masses, springs, and dampers. Simplifications of complex models to simple models are shown in the following sections.

The disadvantage of the latter model was a longer modeling and computational time. Other applications

included modeling of a robotic arm with impact and modeling of industrial cam- follower systems. By creating a dynamic model, the designer can determine the behaviour of a system prior to expensive manufacture, assembly, and testing. If the requirements are not met, appropriate fundamental changes may be made early in the product cycle to obtain acceptable behaviour.

A single degree of freedom (SDOF) model is the simplest dynamic model. An SDOF model can have one or two lumped masses and is typically used as a quick approximation of the dynamic behavior of a system prior to increasing the complexity of the model for a more accurate analysis.

$$\ddot{x} + 2\zeta_{n\_1}\omega_{n\_1}\dot{x} + \omega_{n\_1}^2 x = \frac{1}{M}F(t) \qquad \text{Equation 4}$$

$$\ddot{x} + 2\zeta_{n\_2}\omega_{n\_2}\dot{x} + \omega_{n\_2}^2 x = \frac{1}{M}F(t) \qquad \text{Equation 5}$$

$$\ddot{x} + 2\zeta_{n\_2}\omega_{n\_2}\dot{x} + \omega_{n\_2}^2 x = \frac{1}{M}F(t) \qquad \text{Equation 6}$$

where $x, \dot{x}, \ddot{x}$ are the displacement, velocity and acceleration of M relative to cam follower or $Y - y, \dot{Y} - \dot{y}$, and $\ddot{Y} - \ddot{y}$, respectively and ζ_i are the critical damping factors. The critical damping factors for three masses are represented in Equation 7 to 9.

$$\zeta_1 = \frac{b+\beta}{2M\omega_{n\_1}} \qquad \text{Equation 7}$$

$$\zeta_2 = \frac{\beta}{2M\omega_{n\_2}} \qquad \text{Equation 8}$$

$$\zeta_3 = \frac{b+\beta}{2M\omega_{n\_2}} \qquad \text{Equation 9}$$

where $\zeta_1, \zeta_2, \zeta_3$ shows critical damping factors for the three mass under study. Equations 4, 5, 6 can be applied when y>0 (valve opening), 0 y< (valve closing), and x<0 (valve jumps), respectively. The variable x represents the displacement of mass M with respect to equivalent cam. Barkan's work proved the validity of a mathematical model when he compared the simulated results with the experimental result. Other works that followed tried to improve upon different aspects of the modeling in attempt to increase accuracy or obtain a better understanding of the problems.

where $\zeta_1, \zeta_2, \zeta_3$ shows critical damping factors for the three mass under study. Equations 4, 5, 6 can be applied

when y>0 (valve opening), 0 y< (valve closing), and x<0 (valve jumps), respectively. The variable x represents the displacement of mass M with respect to equivalent cam. Barkan's work proved the validity of a mathematical model when he compared the simulated results with the experimental result. Other works that followed tried to improve upon different aspects of the modeling in attempt to increase accuracy or obtain a better understanding of the problems.

were low and internal damping being enough to damp the excitations.

While many researchers have utilized the one-mass SDOF model to perform their analysis, others venture into the two-mass SDOF model and multiple degrees of freedom (MDOF) models the advantage of utilizing a one-mass SDOF model is simplicity. However, a one mass model does not predict the valve jump accurately. An extreme case of inaccuracy of a one-mass SDOF model was presented in 1983 by Mendez-Adriani. They found that after optimizing the system, it was possible for a one-mass SDOF model to operate at any speed without occurrences of jumps, which was not possible in practice. Therefore, a multi-mass model was created to eliminate this possibility.

The addition of the second mass in the SDOF model allowed one to determine the contact force between the cam and follower and obtain a more accurate result. In addition, the two- mass models predict jump more accurately than the one-mass models. While the entire mass of the one-mass model was relocated to the valve head, the masses in the two- mass model were divided and located at the valve head and the follower. The linkages' flexibilities were modeled and included between the two masses, while the valve head spring connected the mass at the valve head to the ground.
The two-mass SDOF model has the following equation of motion and contact force equation using the notation:

Equation 10
$$M\ddot{x} + b\dot{x} + \left[1 + \frac{k}{K} - \frac{\dot{y}}{|\dot{y}|}\varphi\right]Kx = M\ddot{Y} + k(Y + h)$$

Equation 11
$$F_c = b\dot{x} + Kx + \ddot{Y}M_1$$

where x, $\dot{x}$, $\ddot{x}$ are the displacement, velocity, and acceleration of M relative to equivalent cam follower or $Y - y$, $\dot{Y} - \dot{y}$, and $\ddot{Y} - \ddot{y}$, respectively. The coulomb and viscous dampers were utilized because they improve the accuracy of the dynamic model significantly. The benefits of two-mass model over one mass model is: Allows calculation of contact force. Predicts jump more accurately. Gives a more accurate comparison to the experimental data. The disadvantages of the two- mass model were the division of the masses and more complex equations of motion, but the two-mass SDOF model was the best compromise between accuracy and complexity. When the contact force in the two-mass SDOF model reached zero, separation occurred, and the system became a two degree of freedom model or MDOF model.
A multiple degree of freedom model is a dynamic model having two or more degrees of freedom. The higher the degree of freedom, more accurate the simulation will be, at the price of
a longer computation time. To have a realistic computation time as well as acceptable results, simplifications must be made by reducing the complexity of the model. All researchers understood this concept and tried to maximize the accuracy while minimizing the complexity and calculation time. Most of the complexities of the MDOF models of valve trains involve valve spring modeling. The creation of the MDOF model is like that of the SDOF model. Instead of combining masses, spring constants, and dampers into one lumped value, these parameters are divided and lumped into multiple values depending on the level of complexity desired. The increased in complexity allows other modes of vibrations to appear in the simulated result. The first mode of vibration is the dominant mode, SDOF should be used; otherwise, MDOF may be utilized.

Equation 12
$$m_1\ddot{x}_1 + (c_1 + c_2)\dot{x}_1 - c_2\dot{x}_2 + (k_1 + k_2)x_1 - k_2x_2 = c_1\dot{y} + k_1y$$

Equation 13
$$m_2\ddot{x}_2 - c_2\dot{x}_1 + c_2\dot{x}_2 - k_2x_1 + k_2x_2 = 0$$

has the following equation of motions and contact force equation based on FBD in Norton *et*

al.:

$$m_1\ddot{x}_1 + c_1(\dot{x}_1 - \dot{x}_0) - c_2(\dot{x}_2 - \dot{x}_1) + k_1(x_1 - x_0) - k_2(x_2 - x_1) = 0 \quad \text{Equation 14}$$

$$m_2\ddot{x}_2 + c_2(\dot{x}_2 - \dot{x}_1) + k_2(x_2 - x_1) = 0 \quad \text{Equation 15}$$

$$F_c = m_0\ddot{x}_0 + c_0\dot{x}_0 - c_1(\dot{x}_1 - \dot{x}_0) + k_0x_0 - k_1(x_1 - x_0) + F_i \quad \text{Equation 16}$$

i. MDOF models allow more accurate data to be obtained when compared to the SDOF model. Data such as stresses and loads in the linkages are obtained with an MDOF. The MDOF model should be utilized when the first mode of vibration is not predominant, or a higher degree of accuracy is required. The benefits of an MDOF model over an SDOF model are: Predict the dynamic behavior more accurately.

ii. Allow calculations of stresses between linkages.

Impact modeling is the modeling of impact force that occurs due to a collision of a rigid and elastic, or of two elastic bodies. The impact modeling technique shown in the published literature used the Heaviside step function, which was easily implemented and gave accurate results. The valve-seat was represented by a stiffness constant and viscous damping in the dynamic model.

Based on the reviewed literature, although some studies incorporate CAD tools like SolidWorks for model development, integration of dynamic simulations with fatigue and impact analysis tools, such as MATLAB/Simulink, for a holistic analysis remains a gap. This gap forms the objective of this research.

II. Materials and Methods

The materials used for this research include the following:

Cam-Follower System Components:

a. Cams**:** Various cam profiles (flat, cylindrical, and roller cams) were used to analyze the influence of geometry on system behavior.
b. Followers: Hardened steel and alloy steel followers were selected due to their common application in high-stress environments.
c. Bearings and Shafts**:** High-quality components were employed to ensure smooth operation during testing.

d. High-strength steel alloys (e.g., AISI 4140 and 8620) for the cam and follower materials.

e. Surface-treated samples (e.g., nitriding and carburizing) for analyzing wear and fatigue resistance.
f. Industrial-grade lubricants to simulate real-world operating conditions and minimize friction- induced errors.

Computational Tools: The simulation of the cam-follower behaviour was conducted using MATLAB Simulink. MATLAB Simulink was chosen due to its robust environment for modeling dynamic systems, its built-in solvers for differential equations, and its capability to visualize the results.

2.1 Experimental Equipment

The machine that was used for this work is the Cam Dynamics Test Machine (CDTM) in the Mechanical Engineering Laboratory 1 in University of Uyo, Akwa Ibom State. The output data were divided into three groups; shaft data, primary cam, and secondary cam. The output signals of the shaft data have driveshaft position, torque, and camshaft position, while the output signals for primary and secondary cams are positions, velocities, and accelerations as depicted in Figure 2.

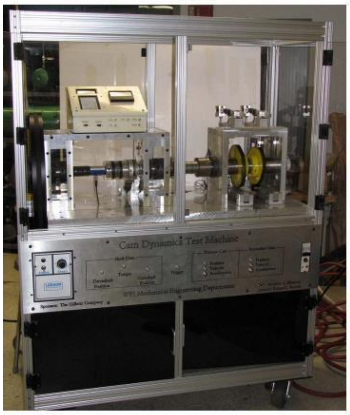

Figure 2: Overview of CDTM

2.2 Method

The research was conducted in three main phases: computational modeling, experimental testing, and data analysis. The following assumptions were considered:

i. The cam and follower are perfectly rigid.
ii. Frictional losses are negligible.
iii. The spring follows Hooke's law.
iv. The impact loads are applied uniformly.

2.2.1 Modelling of CDTM

Once the best impact force approximation was found thorough derivations of the new dynamic model was performed. A few assumptions were made to simplify the problem; these assumptions were that mass M1was always in contact with the cam, the preload force of the spring K23 maintained contact between the impact mass M3 and the intermediate mass M2 up to the point of impact, and the condition of impact did not change from wear caused by multiple impacts. With these assumptions, detailed derivations of the dynamic model were performed for three possible conditions and are presented and discussed in this section.
Besides, dynamic modeling is essential for understanding the response of the system under different operational conditions, ensuring performance optimization and failure prevention. In this study, three critical dynamic phenomena—no contact**,** impact**,** and over-travel—were considered, each representing a unique challenge in cam dynamic.

The Universal Schematic and Free Body Diagram of a cam dynamic test machine represent the physical and dynamic elements of the machine used for studying the behavior of cam-follower systems under dynamic conditions such as impact**,** vibration**,** and fatigue as shown in Figure 3.

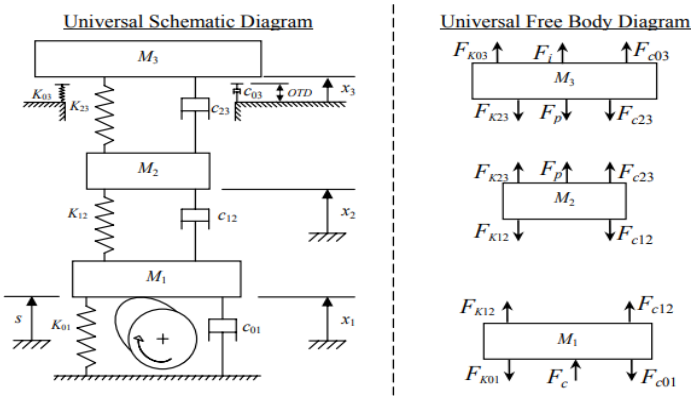

Figure 3: Universal Diagram of CDTM

Also, the Free Body Diagram was used to model and analyze the forces acting on each component of the system, typically the follower and camshaft**.** F_i Result from the acceleration of the follower, where (m) is its mass and $\ddot{x}$is the acceleration as expressed in Equation 17.

$F_i = m\ddot{x}$ Equation 17

A Universal Schematic and Free Body Diagram (FBD) of cam dynamics test machine with no contact typically represent the essential components and forces acting on the system; since the system has no contact, it involves cases where the follower momentarily loses contact with the cam surface due to high speeds, improper spring tension, or system dynamics. Contact is lost when $F_i > F_k + F_c$ and $F_{cam} = 0$; in other way when contact exists, $F_{cam} = k_h\delta^{1.5}$ (Hertzian contact theory). This typically happens at high camshaft speeds or when the spring is too weak. Figure 4 shows the FBD of the CDTM in the first condition which is valid only when the impact mass M3is not in contact with the seat, x2= x3> OTD, where OTD is a fixed predefined over-travel distance.

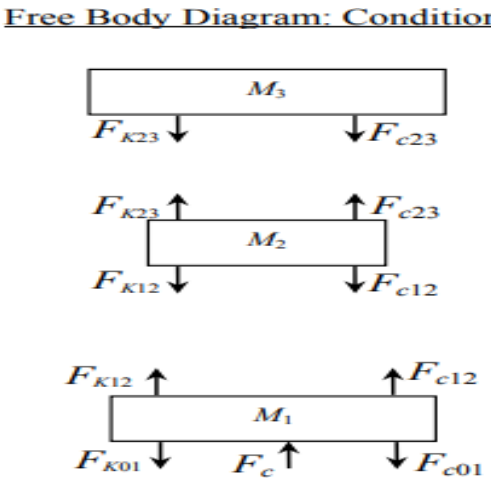

Figure 4: Free body Diagram of CDTM showing Condition 1

The forces acting on the system in this condition can be divided into three categories; contact force (Fc), spring force (Fkij), and damping force (Fcij) where ij represents the subscripts of the spring constants and damping coefficients. From the FBD shown in Figure 5, equations of motion were derived:

$$\sum F_{M1} = F_{k12} + F_{c12} + F_c - F_{k01} - F_{c01} = m_1\ddot{x_1} \quad \text{Equation 18}$$

$$\sum F_{M2} = F_{k23} + F_{c23} - F_{k12} - F_{c12} = m_2\ddot{x_2} \quad \text{Equation 19}$$

$\sum F_{M3} = -F_{k23} - F_{c23} = m_3\ddot{x_3}$ Equation 20 a

where:

$F_{k01} = k_{01}(x_1)$ Equation 21 b $\quad F_{c01} = C_{01}(\dot{x_1})$ Equation 21 c

$F_{k12} = k_{12}(x_2 - x_1)$ Equation 21 d $\quad F_{c12} = C_{12}(\dot{x_2} - \dot{x_1})$ Equation 21 e

$F_{k23} = F_{k23-push} = k_{23}(x_3 - x_2) F_{c23} = C_{23}(\dot{x_3} - \dot{x_2})$ Equation 21 f

The impact case occurs when the follower, after losing contact, re-establishes contact with the cam surface. This can lead to high impact forces, vibrations, and potential damage to the system. The next condition took place at the instant the impact mass M3 struck the seat, x2=x3= OTD. From this condition, a new FBD was developed and shown in Figure 5.

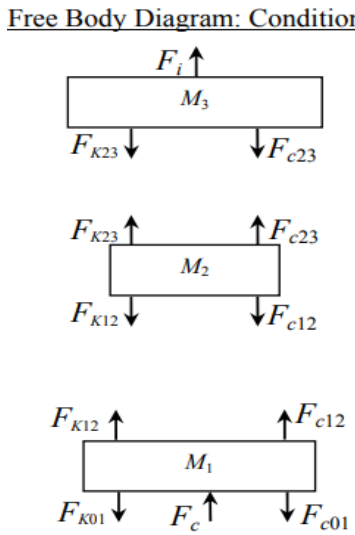

Figure 5: Diagram of CDTM: Condition 2

The forces acting on the system under this condition and can be divided into four categories; contact force (F_c), spring force (F_{kij}), damping force (F_{cij}), and impact force.

(F_i). From the FBD shown in Figure 6, Equations of motion were derived:

$$\sum F_{M1} = F_{k12} + F_{c12} + F_c - F_{k01} - F_{c01} = m_1\ddot{x}_1 \quad \text{Equation 21}$$

$$\sum F_{M2} = F_{k23} + F_{c23} - F_{k12} - F_{c12} = m_2\ddot{x}_2 \quad \text{Equation 22}$$

$$\sum F_{M3} = F_1 - F_{k23} - F_{c23} = m_3\ddot{x}_3 \quad \text{Equation 23}$$

where:

$F_{k01} = k_{01}(x_1)$ Equation 24

$F_{c01} = C_{01}(\dot{x}_1)$ Equation 25

$F_{k12} = k_{12}(x_2 - x_1)$ Equation 26 $F_{c12} = C_{12}(\dot{x}_2 - \dot{x}_1)$ Equation 27

$F_{k23} = F_{k23-push} = k_{23}(x_3 - x_2)$ Equation 28 $F_{c23} = C_{23}(\dot{x}_3 - \dot{x}_2)$ Equation 29

$F_i = C^I/(a+1)\{\frac{a+1}{2} m_2(v_{1-}v_2)^{2(a/a+1)}\}$ Equation 30

However, with the above equations of motion, impact force was calculated and satisfied the impact modeling requirement. The missing component of the new dynamic model will be the over travel which is shown below.

Over-travel occurs when the follower motion exceeds the designed travel range, often due to excessive cam speeds or improper spring design. This can lead to mechanical interference, stress concentrations, and fatigue failure. Over-travel was modeled as an additional constraint on the follower displacement, beyond which contact, or interference occurs. The system's dynamic response and failure points were analyzed for varying camshaft speeds and spring stiffness.

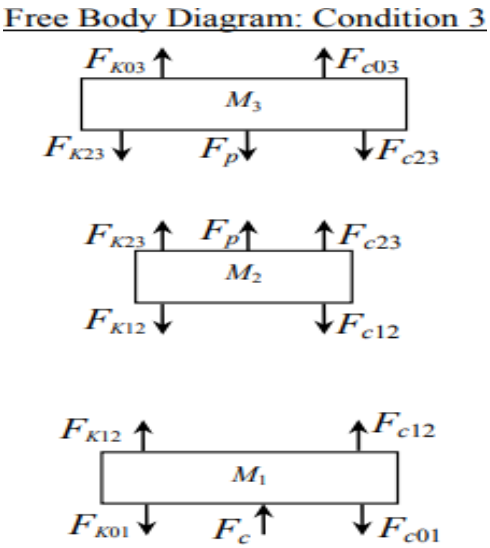

Figure 6: FBD of CDTM for Condition 3–Over-Travel

Figure 6 shows the FBD for the third condition which applies when the impact mass M_3 and intermediate mass M_2 separates, $x_2 < x_3 <$ OTD. During the separation, the fixed preload force of the spring Fp tries to pull the two masses back together as shown in the FBD in Figure 6. The forces acting under this condition will be divided into

four categories: contact force (Fc), spring force (F_{kij}), damping force (F_{cij}), and preload force (F_p). From the above FBD, the last equations of motion for the CDTM were developed and shown below.

$\sum F_{M1} = F_{k12} + F_{c12} + F_c - F_{k01} - F_{c01} = m_1\ddot{x}_1$ Equation 31

$\sum F_{M2} = F_{k23} + F_{c23} + F_p - F_{k12} - F_{c12} = m_2\ddot{x}_2$ Equation 32

$\sum F_{M3} = F_{k03} - F_{c03} - F_{k23} - F_{c23} - F_p = m_3\ddot{x}_3$ Equation 33

where:

$F_{k01} = k_{01}(x_1)$ Equation 34
$F_{c01} = C_{01}(\dot{x}_1)$ Equation 35

$F_{k12} = k_{12}(x_2 - x_1)$ Equation 36

$F_{c12} = C_{12}(\dot{x}_2 - \dot{x}_1)$ Equation 37

$F_{k23} = F_{k23-push} = k_{23}(x_3 - x_2)$ Equation 38

$F_{c23} = C_{23}(\dot{x}_3 - \dot{x}_2)$ Equation 39

$F_{k03} = k_{o3}(OTD - x_3)$ Equation 40

$F_{k03} = C_{03}(\dot{x}_3)$ Equation 41

2.2.2 Dynamic Simulations Model Using MATLAB/Simulink

MATLAB/Simulink was used to simulate the dynamic response of the cam-follower system. Parameters such as cam speed, load amplitude, and contact forces were varied to study their influence on system behaviour. The simulation modeled took into consideration the following:

i. Impact loads as sudden force applications during cam operation.

ii. Fatigue loads as cyclic forces acting over extended periods.

More so, the dynamic model incorporated Contact Forces which was modeled using Hertzian contact theory; Damping and Stiffness, modeled and represented as system parameters in the Simulink blocks; Vibration Analysis, simulated to predict system stability and resonance conditions. Table presents MATLAB/Simulink input parameters for system conditions.

Table 1. MATLAB/Simulink input parameters that reflect the system rating conditions.

Parameter	Symbol	Value	Unit	Description
Follower Length	l	0.6	Meters	Length of the follower component.
Follower Radius	r	0.005	Meters	Radius of the follower.
Follower Mass	m	0.3676	Kilograms	Mass of the follower.
Cam Radius	R	0.09	Meters	Base radius of the cam.
Cam Eccentricity	e	0.04	meters	Offset distance between the cam's rotation axis and its geometric center.
Poisson's Ratio	ν	0.3	-	Material property indicating the ratio of transverse strain to axial strain.
Acceleration Due to Gravity	g	9.81	m/s²	Standard acceleration due to gravity.
Friction Coefficient	μf	0.3	-	Coefficient of friction between the cam and follower surfaces.

Impact Damping Factor	β	3.25	s/m	Damping factor accounting for energy dissipation during impact.
Impact Recovery Coefficient	ξ	0.42	-	Coefficient representing the restitution characteristic after impact.
Modulus of Elasticity	Y	2.07×10^{11}	Pascals	Young's modulus of the material, indicating stiffness.
Cam Angular Velocity	ω	28.7	rad/s	Rotational speed of the cam.

[17]

To establish the simulation, the system was first defined**,** MATLAB/Simulink blocks were used to build the cam-follower system. The Rotational Motion Block was modeled using a Sine Wave block or a custom input signal which represented the cam profile's displacement over time. The cam's angular velocity (ω) and eccentricity (e) determined the profile's characteristics. The follower's response for Mass-Spring-Damper System was model using the Mass (m), Spring Stiffness (k), and Damping Coefficient (c). These was Implemented using Simulink's Mass- Spring-Damper blocks.
For the Contact Forces Hertzian Contact Theory was used to compute contact forces (Fc).

Simulink custom blocks or MATLAB Function blocks was computed with Equation 42.

$Fc = k(\Delta)^n - c \times \dot{\Delta}$ Equation 42

where Δ is the deformation and $\dot{\Delta}$ is the deformation rate. Friction Effects used a friction Model using Coulomb friction as shown in Equation 43.

$F_f = \mu_f \times F_n$ Equation 43

2.3 System modeling

A mathematical model of the cam-follower system was developed to simulate its dynamic behavior under impact and fatigue loading. The model includes:

Kinematics focuses on the motion of the follower without considering forces. The motion of the cam governs the follower displacement, velocity, and acceleration.

The follower's displacement (x(t)) depends on the cam profile. Common cam profiles include simple harmonic motion (SHM), cycloidal motion, or parabolic motion as expressed in Equation 44.
For SHM:

$$x(t) = h\,(1 - cos\,\left(\frac{\pi t}{T}\right)) \quad \text{Equation 44}$$

where: h is lift or rise of the follower and T is time for one cam revolution.

Velocity equation which is the first derivative of displacement with respect to time was modeled as expressed in Equation 45.

$$v(t) = \frac{dx(t)}{dt} = \frac{h}{T}\sin\,(\frac{\pi t}{T}) \quad \text{Equation 45}$$

$$a(t) = \frac{d^2x(t)}{dt^2} - \frac{h\pi^2}{T^2}\cos\,(\frac{\pi t}{T}) \quad \text{Equation 46}$$

The dynamic analysis involves the forces acting on the follower and the resulting motion.

The forces acting on the follower are:

Spring Force(F_k) = $kx(t)$ Equation 47 where k is the spring constant

The damping force

$$F_c = c\frac{dx(t)}{dt}$$ Equation 48

where c is the damping constant.

The inertia force

$$F_i = m\frac{d^2x}{dt^2}$$ Equation 49

where m is the mass of the follower The total force (F) is:

$$F = F_k + F_c + F_i$$ Equation 50

Using Newton's Second Law (F = ma), the equation of motion for the cam-follower system becomes:

$$m\frac{d^2x}{dt^2} + c\frac{dx}{dt} + k(x - x_o) = F_{cam} + F_{impact}$$ Equation 51

where m is Follower mass, c is Damping coefficient, k is Spring stiffness, x is Follower displacement, F_{cam} is Cam contact force and F_{impact} is External impact force. To reiterate the contact forces (Hertzian contact theory) was used to compute contact forces (F_{cam}) as shown in Equation 52.

$$F_{cam} = k_h\delta^{1.5}$$ Equation 52

where k_h is Hertzian stiffness constant (depends on material properties and contact geometry), δ is Elastic deformation.

The Fatigue Life Estimation was modeled using the S-N curve approach as shown in Equation 53

$$\frac{\partial_{max}}{\partial_{endurance}} = N(1 - R)$$ Equation 53

where σ_{max} is Maximum stress, $\sigma_{endurance}$ is Endurance stress limit, N is Number of cycles to failure and R is Stress ratio.

Combining the forces acting on the follower into the governing differential equation, Equation 54 was derived.

$$m\frac{d^2x}{dt^2} + c\frac{dx}{dt} + kx = F_{cam}$$ Equation 54

Impact force model for short-duration impacts was computed with Equation 55.

$$\bar{F_{impact}}(t) = \frac{1}{2}v^2A$$ Equation 55

where ρ is Density of the impacting material, v is Relative velocity at impact and A is Contact area. Fatigue Damage Accumulation was computed using Miner's Rule as shown in Equation 56.

$$D = \sum\frac{n_i}{N_i}$$ Equation 56

where D is Damage fraction, n_i is Number of cycles applied at stress level i and N_i is Number of cycles to failure at stress level i.

There are multiple methods in finding solutions of differential equations. The two methods that are discussed in this study are the state space and block diagram methods. State space uses a set of first order differential equations to describe the system of interest, which typically require the end-user to convert the system to conform to the required format. These consist of writing the equations of motion in terms of state variables and place these variables in state equation. Once the state equation has been finalized, the system must be placed in a state space form which is written in standard matrix format. This process may be easily performed for a one mass, one damper, and one spring system, it becomes rather complex for a higher degree of freedom model for an inexperience user. While state space is easy to use for a simple system, a block diagram is always simpler regardless of the complexity of the problem. Table 2 shows a simplified CDTM 3- mass 2-DOF with parameters.

Table 2: Simplified CDTM: 3-Mass 2-DOF with calculated parameters

Variable	Definition	Summation	value
$M1$	Follower mass	$ma+mcr$	7.42kg
$M2$	Intermediate mass	$marr+marl+mbre$	0.7433kg
$M3$	Impact mass	$Mbre$	0.1748kg
$K01$	Ground to M1 stiffness	$kcs+kcr$	4,486.8kg/m
$K12$	$M1$ to $M2$ stiffness	$kcr+karr$	1,585,072.98 kg/m
$K23$	$M2$ to$M3$ stiffness	$karl+kbre$	1,426,232.94 kg/m
$K03$	Ground to $M3$ stiffness	-	8,598,902.73 kg/m
OTD	Over-travel-Distance	-	0.0015625m
Preload	$K23$(Die Spring) Preload	-	12.767kg

[18]

State space requires the end-user to transform the differential equations of motion into state space form.

2.4 Block diagram: Matlab and Simulink

Huang *et al.* (2013), presented a 3 mass 2-DOF model with four main inputs. The block diagram develop for this research work are presented in Figures 7, 8, 9, 10, 11, 12 and 13 respectively.

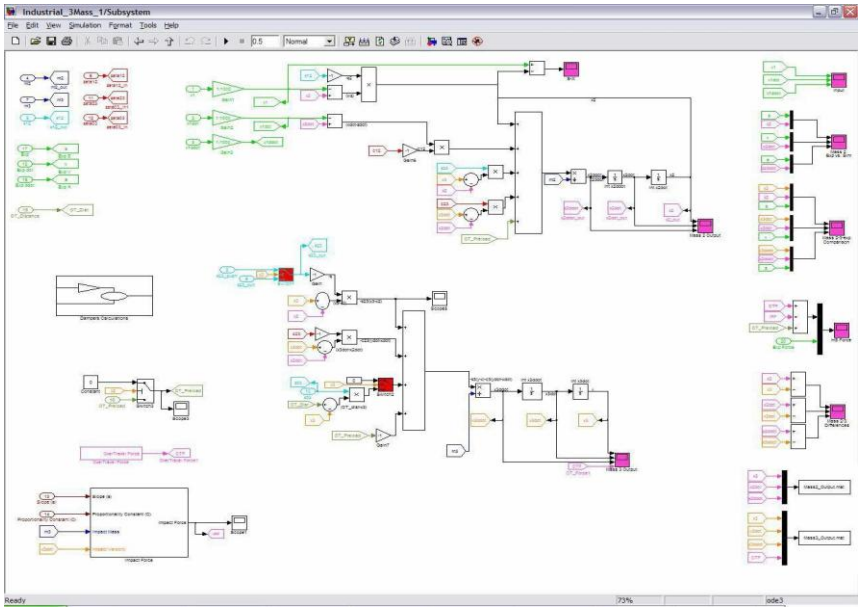

Figure 7: Simulink's Sub-System of 3-Mass 2-DOF Industrial Model

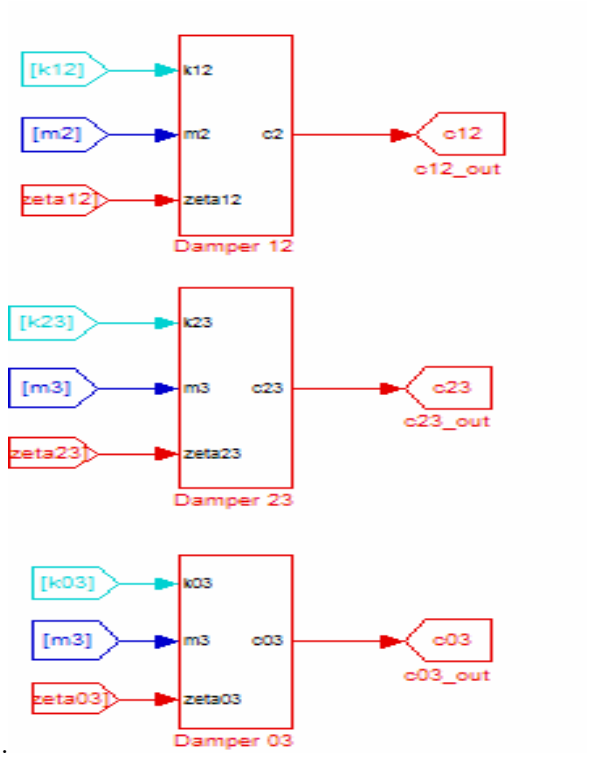

Figure 8: Sub-Section 2: Damping Calculation for 3-Mass 2-DOF Model

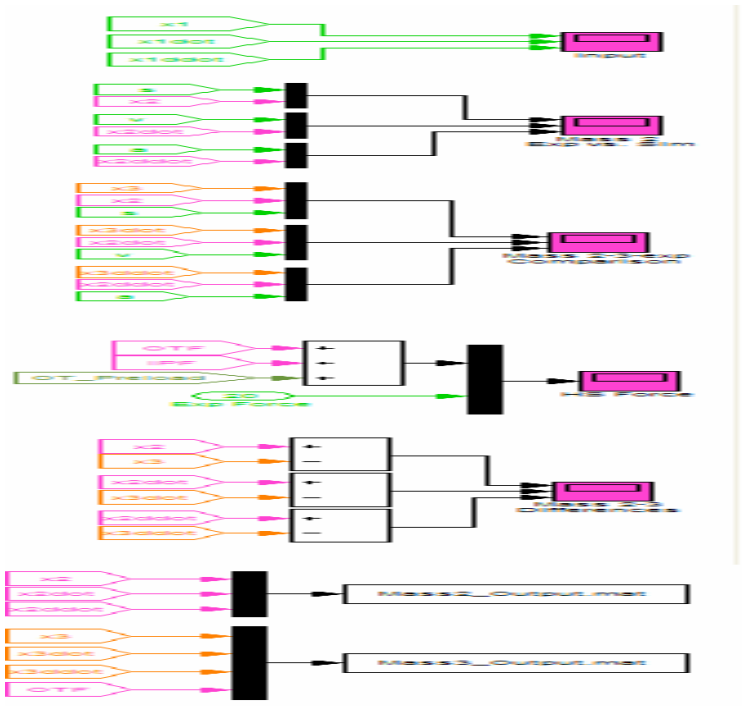

Figure 9: Sub-Section5: Results

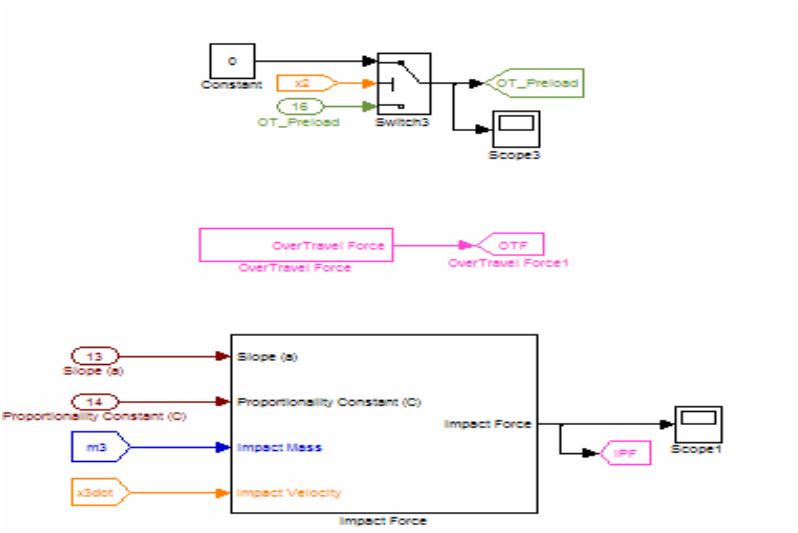

Figure 10: Sub-Section 3: Force Determinations

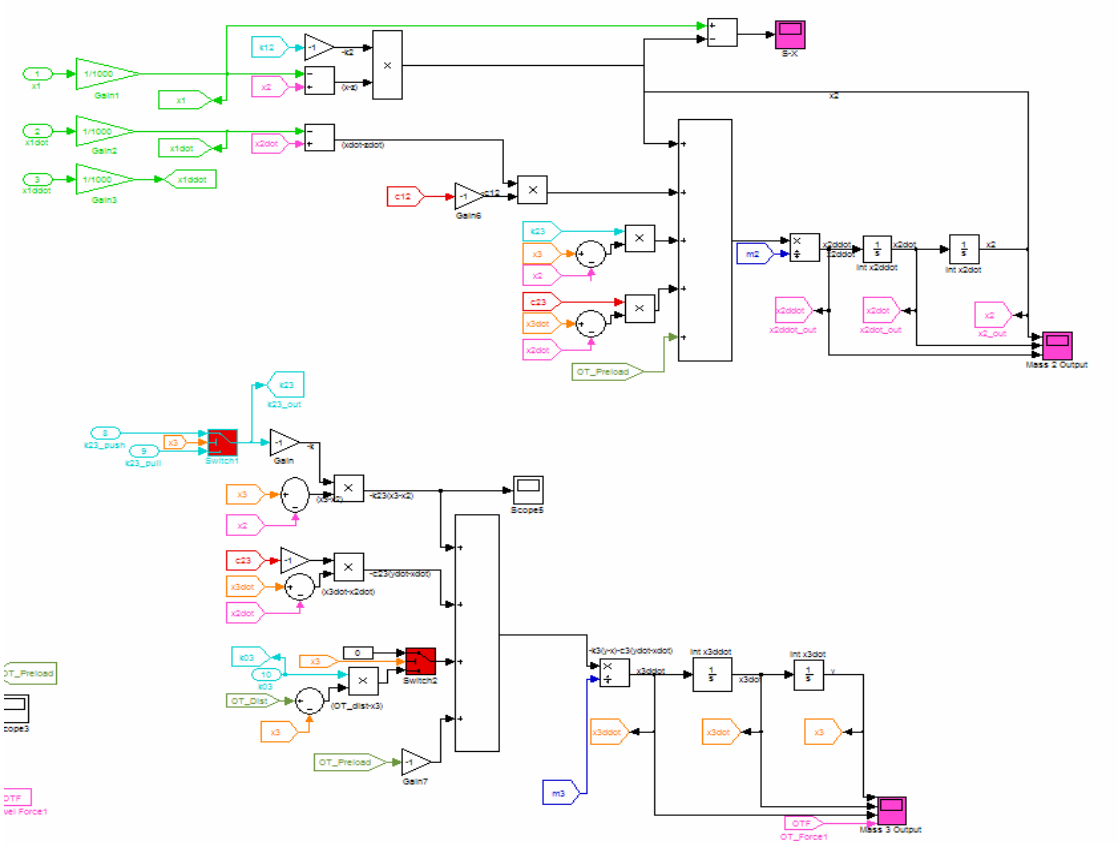

Figure 11: Sub-Section4: Equations of Motion

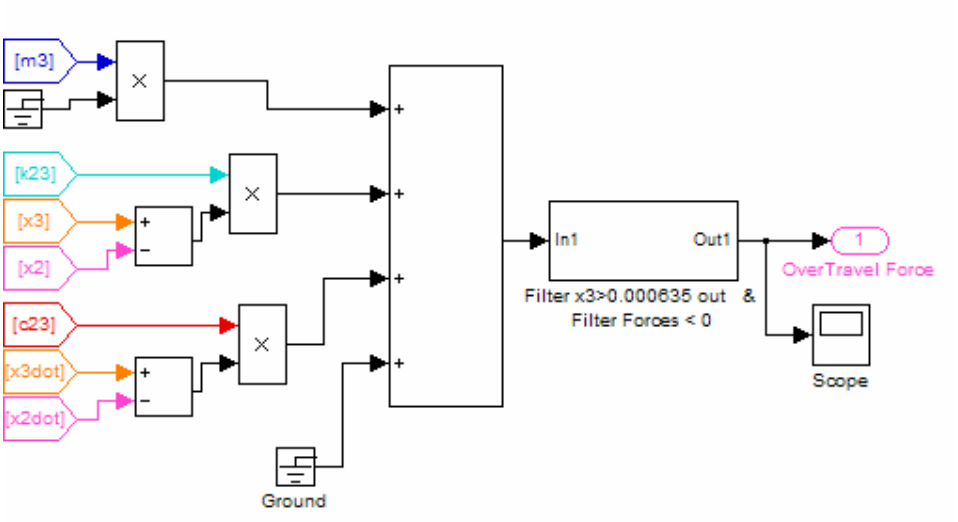

Figure 12: Over-Travel Force Calculation for3-Mass2-DOF Model

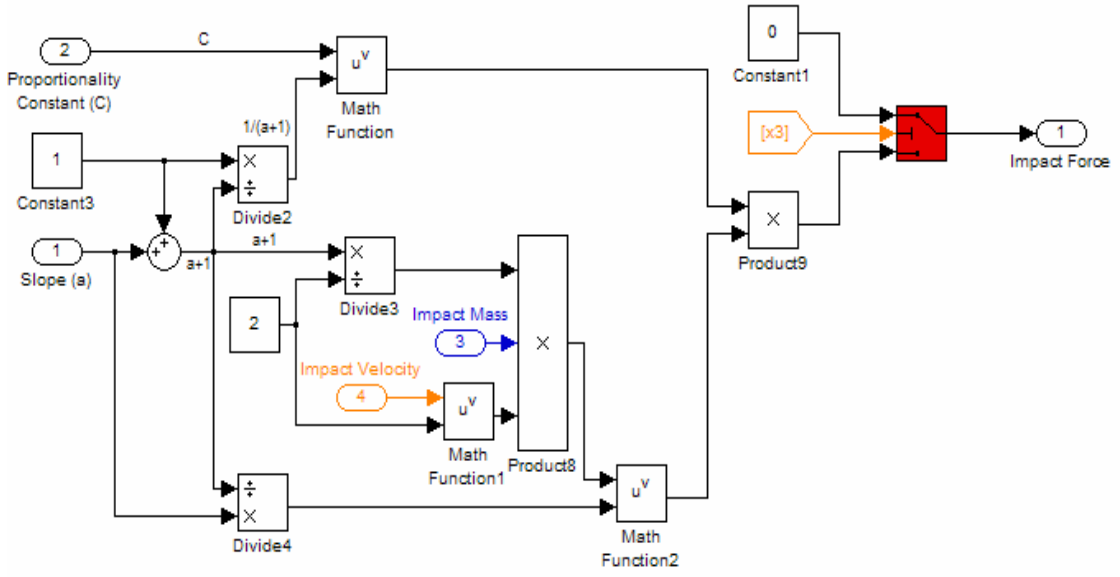

Figure 13: Impact Force Calculation for 3-Mass 2-DOF Model

III. Results and Discussion

3.1 Results

Figure 14 shows a replicate of the schematic diagram of the intermediate mass, M_2, and the impact mass, M_3; their simulated displacement comparison shown in Figure 15.

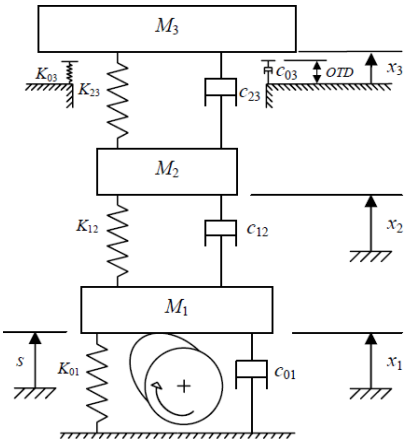

Figure 14: CDTM Equivalent 3-Mass 2-DOF Schematic Diagram

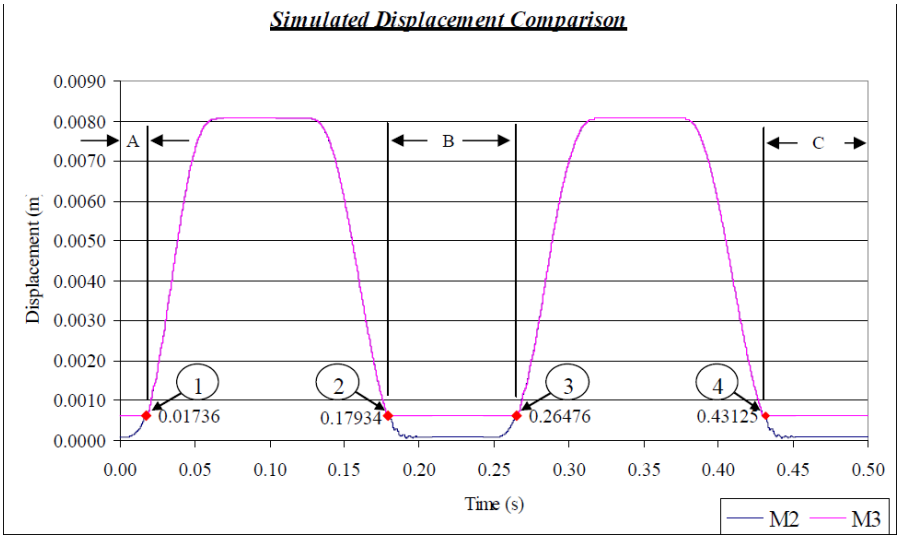

Figure 15: Simulated Displacement Comparison of *M*2 and *M*3

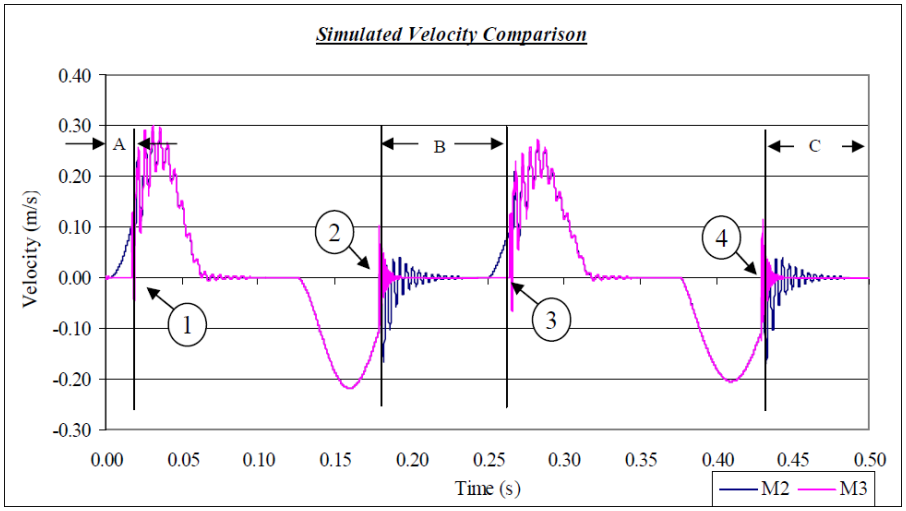

Figure 16: Simulated Velocity Comparison of *M*2 and *M*3

Figure 17 and Figure 18 represent plot for vibration for *M*2 and *M*3 after the second impact

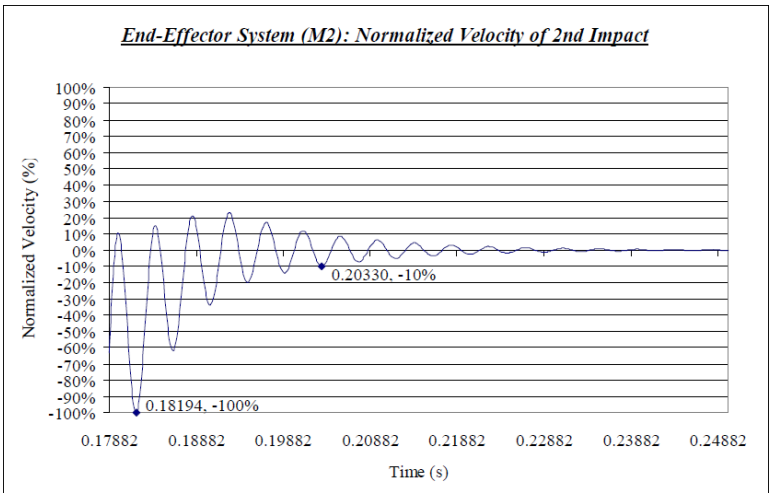

Figure 17: Normalized Simulated Velocity of M2 after the 2nd Impact

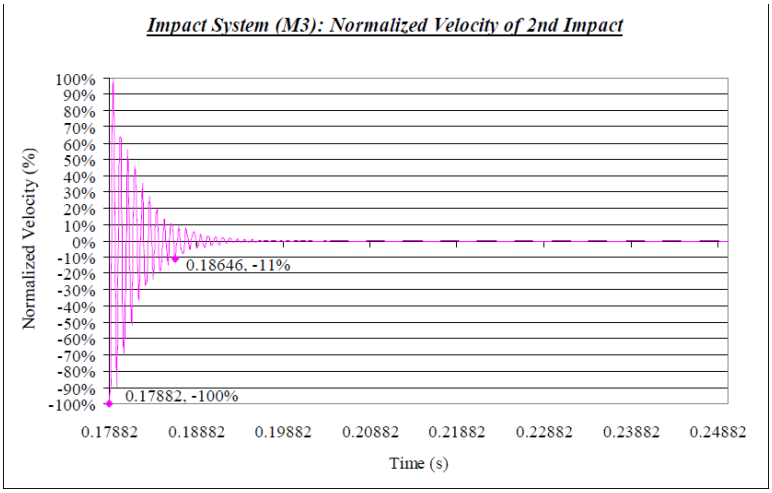

Figure 18: Normalized Simulated Velocity of *M*3 after the 2nd Impact

In Figure 17 and Figure 18 two data points were marked and labeled with the maximum amplitude of vibration, the point of ten percentage of the maximum after the second impact, and the time at which these events occurred. These data points were used to determine a measure of the impact period for *M*2 and *M*3. *M*2 took 0.02136s (0.20330s – 0.18194s) for the magnitude of vibration to reduce to 10% of the maximum and *M*3 took 0.007639s (0.18646s – 0.17882s) for the same reduction to occur.

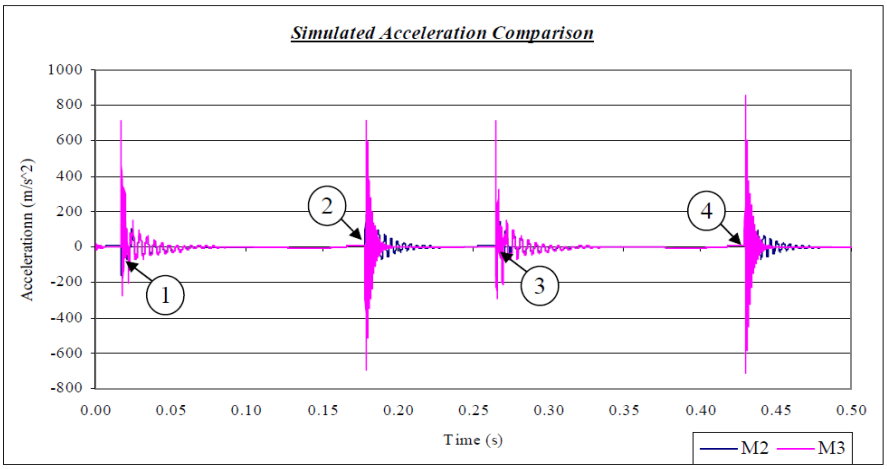

Figure 19: Simulated Acceleration Comparison of *m*2 and *m*3 So

Figure 19 shows the simulated accelerations of masses *M*2 and *M*3. As expected, the magnitude of the vibration of *M*3 is 4 to 5 times greater than that of *M*2 because that is the location where impacts occur.
Figure 20 shows the simulated force as a result of *M*3 striking the force transducer. It also represents the sum of three forces which are impact, preload, and over-travel forces.

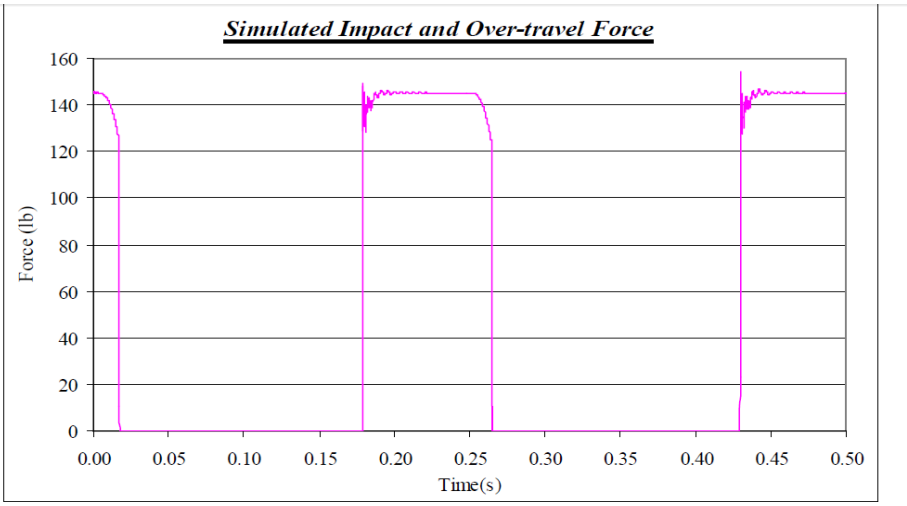

Figure 20: Simulated Impact and Over-travel Force

4.2. Discussion

From Figure 15 the displacement profile exhibits a periodic nature, with an initial rise (A), a sustained peak displacement (B), and a decline (C), correlating with the cam rotation. The transition points (1, 2, 3, and 4) indicate critical time instances where displacement changes significantly. The influence of masses M1 and M2 is evident in the response characteristics. A larger mass tends to reduce follower acceleration, leading to smoother transitions but increased inertia effects. The response for M2 (higher mass) exhibits delayed transitions compared to M1, implying a potential trade-off between stability and responsiveness. The peak displacement remains similar for both masses, suggesting that the cam profile dictates the maximum displacement while mass primarily affects the dynamic response timing. However, the displacement graph presents a comparison of the follower's motion under different mass conditions. The periodic nature of the graph confirms the expected cam profile behavior, where the follower undergoes a rise phase, dwell phase, and return phase. The displacement remains relatively consistent across the cycles, indicating that the cam's design is the primary determinant of displacement. However, mass variations introduce slight delays in the transitions due to inertia.

affecting the timing and precision of the follower's response. In practical applications, these observations suggest that selecting an appropriate mass is crucial to maintaining synchronization with the camshaft's motion, particularly in high-speed mechanisms where timing precision is critical.
More so the graphical result in Figure 16 connotes that M2 and M3 exhibit alternating velocity changes, with velocity peaks reaching about 0.3 m/s in both positive and negative directions. The alternating nature confirms energy transfer between masses. The presence of phases (marked A, B, C) suggests different stages of impact, rebound, and damping. In addition, from the results from Figure 16, comparing velocity trends of M2 and M3 revealed the interplay between mass and momentum transfer. M2, as an intermediate mass, undergoes velocity fluctuations due to repeated energy exchanges. In contrast, M3, acting as a more terminal mass, exhibits a relatively smoother deceleration profile. The phase shift between velocity curves indicates differential energy absorption and transfer rates. From the graphical result in Figure 17 and Similar to M2, M3 experiences a sharp velocity drop, reaching -100% at t = 0.17882s. The velocity oscillates and stabilizes around -11% at t = 0.18646s. Compared to M2, the damping effect is slightly faster, indicating differences in mass or damping properties. The velocity profiles of M2 and M3 after the second impact reveal key insights into the system's dynamic response. The normalized velocity trends indicate a significant change post-impact, suggesting that energy transfer between masses follows an expected pattern. The deceleration and subsequent oscillations imply a redistribution of momentum, potentially influenced by system damping and impact elasticity. Considering result from Figure 18, Similar to M2, M3 experiences a sharp velocity drop, reaching -100% at t = 0.17882s. The velocity oscillates and stabilizes around -11% at t = 0.18646s. Compared to M2, the damping effect is slightly faster, indicating differences in mass or damping properties. As observed in Figure 19**,** distinct peaks in acceleration were observed at four major impact events.

The acceleration for M2 reaches about ±800 m/s^2, while M3 undergoes a similar magnitude but slightly lower peak values. This suggests that M2 undergoes stronger impulsive forces compared to M3, which aligns with its higher initial velocity. In detail the acceleration profiles of M2 and M3 demonstrate transient peaks, which correspond to the moments of impact and energy dissipation through the system. M2 exhibits a more fluctuating acceleration curve, indicative of intermediate interactions between impacting masses. On the other hand, M3 shows a relatively smoother transition, suggesting its role as a terminal mass in the energy dissipation sequence. The discrepancies in acceleration amplitude implied differences in mass ratios and structural constraints within the simulated environment.
Considering the Simulated Impact and Over-Travel Force in Figure 20 the force exerted during impacts peaks was at approximately 63.50293 -68.03886 kg. The force-time profile exhibits periodic force applications at approximately 0.15s intervals. This pattern suggests a cyclic impact behavior, possibly due to repetitive bouncing effects after the initial impact.

Validation of the results
More so, the acceleration trends observed align with validated models in literature, notably in [16], where comparable dynamic systems exhibited acceleration profiles within 10– 15% of experimental error bounds. Similarly,

In the "Impact" scenario, the system experiences sharp acceleration spikes—approaching ±200 m/s²— followed by high-frequency, exponentially decaying oscillations. These responses occur periodically at around 0.00 s, 0.17 s, 0.30 s, and 0.43 s, clearly showing the effect of repeated impacts. [20] emphasized that systems subjected to impact forces exhibit immediate and sharp acceleration peaks, which gradually decay as energy dissipates through system damping.

IV. Conclusion

The common velocity method overestimated the impact forces by10% to 25% whereas the energy method underestimated the impact forces by 35% to 40%. Another discovery was the inadequacy of the two-mass SDOF model for a cam-follower system with impact and over-travel.

References

[1] Shigleys Mechanical Engineering Design. NewYork: McGraw-Hill, 265-344.
[2] Patel, N. S. (2015). Modelling, Design and Analysis of Cam and Follower-A Review Paper.
[3] Chaboche, J. (1988), Continuum damage mechanics and its application to structural lifetime prediction, Rech. Aerosp, 4, 37-53.
[4] Chang, W. T. and Long-Iong, W. (2009). A computerized approach for tolerance analysis of disk cam mechanisms with a flat-faced follower. *Transactions of the Canadian Society for Mechanical Engineering*, 33(3): 459-485.
[5] Chang, W. T. and Long-Iong, W. (2009). Computerized tolerance analysis of disk cam mechanisms with a roller follower. *Engineering with Computers,* 25: 247-260.
[6] Cui, W. C. (2002). A state-of-the-art review on fatigue life prediction methods for metal structures. *Journal of Marine Science and Technology*, 7(1): 43–56.
[7] Pieringer, A., Kropp, W. and Nielsen, J. C. O. (2014), The influence of contact modelling on simulated wheel/rail interaction due to wheel flats wear, 314: 273–281
[8] Dietz, S., Netter, H. and Sachau, D. (1998). Fatigue Life Prediction of a Railway Bogie under Dynamic Loads through Simulation. Vehicle System Dynamics. *International Journal of Vehicle Mechanics and Mobility*, 29(6):385–402.
[9] Dowling, N. E., Calhoun, C.A. and Arcari, A. (2009). Mean stress effects in stress-life fatigue and the walker equation. *Fatigue and Fracture of Engineering Materials and Structures,* 2009, (32): 163–179.
[10] Budynas, R. G. and Nisbett, J. K. (2014).
[11] Miller, K. J. and Zachariah, K. P. (1977). Cumulative damage laws for fatigue crack initiation and stage i propagation. *The Journal of Strain Analysis for Engineering Design*, 12(4), 262-270.
[12] Dattakumar, S. and Ganeshan, V. (2017). *Converting dynamic impact events to equivalent static loads in vehicle chassis*, MSc Dissertation, Chalmers University of Technology, Gothenburg, Sweden, 77p.
[13] Redfield, R.C. and Sutela, C (2012). Mountain bike wheel endurance testing and modeling.
Procedia Engineering, 34: 658-663.
[14] Marques, F., Moutinho, C., Magalhães, F., Caetano, E. and Cunha, Á. (2014). Analysis of Dynamic and Fatigue Effects in an Old Metallic Riveted Bridge. *Journal of constructional steel research*, 99: 85-101
[15] Pozuelo, D., Gauchia, A., Olmeda, E. and Diaz, V (2014). Bump Modeling and Vehicle Vertical Dynamics Prediction. *Advances in Mechanical Engineering*, 6: 736-576.
[16] Han, L., Jing, L. and Liu, K. (2015). A dynamic simulation of the wheel–rail impact caused by a wheel flat using a 3-D rolling contact model. *Journal of Modern Transportation*, 25(2): 124-131.
[17] Deng, Z., and Chen, Y. (2019). Effect of Surface Morphology on Dynamic Characteristics of Cam-Follower Oblique Impact System. Shock and Vibration, 1–12. https://doi.org/10.1155/2019/3956169.
[18] Wang, Linyan, Tao Shen, Yunbo Shen, and Shaokang, L. (2012). Development of Parametric Design System for Disc Cams with Translating Roller Followers. *Advanced Materials Research*, 411: 83-87.
[19]Huang, C., Cheng-Kang, H., Chih-Jie, Y. and Cheng-Kuo, S. (2013). Experimental Investigation on the Performance of a Compressed-Air Driven Piston Engine. *Energies,* 6(3): 1731-1745.
[20] Son, L., Farid, M., Bur, M., & Darmawan. (2023). *Impact response analysis of vibration system with inerter*. Proceedings of the Institution of Mechanical Engineers, Part K: Journal of Multi-body Dynamics. https://doi.org/10.1177/09574565221150184